Advanced Powder Technology xxx (xxxx) xxx

Contents lists available at ScienceDirect

Advanced Powder Technology

journal homepage: www.elsevier.com/locate/apt

Original Research Paper

Triaxial behavior of granular material under complex loading path by a new numerical true triaxial engine

Xiaoliang Wang [a,*], Zhen Zhang [a], Jiachun Li [a,b,*]

[a] Key Laboratory for Mechanics in Fluid Solid Coupling Systems, Institute of Mechanics, Chinese Academy of Sciences, Beijing, China
[b] School of Engineering Science, University of Chinese Academy of Sciences, Beijing 100049, China

ARTICLE INFO

Article history:
Received 5 August 2018
Received in revised form 26 December 2018
Accepted 27 December 2018
Available online xxxx

Keywords:
Granular material
Stress path
Strength criterion
Discrete element method
Numerical true triaxial engine

ABSTRACT

A new numerical true triaxial engine based on discrete element method accounting for rolling resistance contact is developed. By this engine, we have simulated mechanical behavior of granular materials under complex stress loading path in this study. Stress-strain responses of a kind of typical granular sand under several stress loading path in meridian and deviatoric stress space are provided. The results show that the three dimensional effects like the intermediate principal stress play an important role in the modeling processes. Theoretical analysis in strength characteristic implies the strength criteria with three parameters such as unified strength criterion and van Eekelen strength criterion are capable of describing cohesionless granular material behaviors in three dimensional stress states. Moreover, the case study for Chende sand further demonstrates the numerical true triaxial engine, is a potential tool. As compared to conventional triaxial compression test, this new developed apparatus could be widely used to "measure" elastic-plastic behavior in three dimensional stress space for finite element analysis in geotechnical problems.

1. Introduction

Granular material in geotechnical and geological engineering tends to be in complicated three dimensional (3D) stress states. Lots of loading experiments of granular material prove that their stress-strain behavior evidently depends on stress loading path. And thus, the corresponding strength property heavily relies on intermediate principal stress [1]. Researchers have developed true triaxial compression apparatus to deal with these issues. However, it seems to be uneasy to obtain required samples with specified initial state, relative density, and water content et al. In addition, the manipulation of stress loading is even more difficult than those in conventional triaxial compression tests. It is still challenge to bridge the existing wide gap between required rich information in advanced 3D elastic-plastic behavior for FEM analysis and very limited data by geological survey in geotechnical engineering. However, the present numerical triaxial apparatus based on discrete element method (DEM), if well calibrated by tests in simple loading path, could become a potential technique to overcome this bottleneck in real triaxial experiment and geological survey.

The widely used strength criteria of granular materials implemented in some commercial software like ABAQUS, includes Mohr-Coulomb (MC) criterion and Drucker-Prager (DP) criterion. Both of them seem to manifest themselves not so well enough in complex 3D stress loading path. Both Lade-Duncan strength criterion [2] and Matsuoka-Nakai criterion [3] have considered the influence of intermediate principal stress and the anisotropy in deviatoric stress plane. Nevertheless, their mathematical expressions are rather complicated and strongly nonlinear. In contrast, van Eekelen (VE) [4] primarily developed a general but simple strength criterion for granular material with 3D effect considered. Besides, the unified strength theory (UST) criterion proposed by Yu [5] uses piecewise linear functions to model influences of intermediate principal stress, and has already been applied to model the strength of metal, rock, concrete and soil under complex stress states. Naturally, more concise strength criteria with limited number of parameters are expected by FEM researchers in geotechnical engineering.

Discrete element method (DEM), invented by Peter Cundall in 1979 [6], has been extensively used in the study of granular material related fundamental study and engineering applications. Gong et al. [7] simulated consolidated drained compression and

* Corresponding authors at: Key Laboratory for Mechanics in Fluid Solid Coupling Systems, Institute of Mechanics, Chinese Academy of Sciences, Beijing, China (J. Li).
E-mail addresses: wangxiaoliang@imech.ac.cn (X. Wang), jcli05@imech.ac.cn (J. Li).

https://doi.org/10.1016/j.apt.2018.12.020
0921-8831/

undrained plane compression by DEM. Kuhn [8] observed the evolution of microstructures of granular materials along with their indicators during failure. It attracts many people's interests in how to model the effects of non-spherical shape granular materials in reality. Some researchers add a rolling resistance to the spherical particle model by parameterization. Researches in this regard include Iwashita [9], Jiang [10] and Wang [11]. Others have developed a non-spherical particle model, including cluster or clump of spherical particles [12], polygonal particle [13], and ellipsoid particle [14] and also their contact detection algorithm. In addition, Scholtès [15], Wang [16] further developed liquid bridge model to simulate behavior of unsaturated granular materials.

Zhao [17] studied the critical state characteristics of granular materials with different initial porosities by conventional triaxial compression, plane strain shear and direct shear test through the commercial software PFC3D, where only spherical particle packing and simple loading in either plane stress or symmetric loading were concerned with. Ng [14,18] used his own in-house DEM code ELLIPSE3H to generate three different initial samples, and then simulated consolidated drained compression, axial extension, constant mean pressure compression, lateral compression and lateral extension in meridian stress space. He obtained the stress-strain response and strength characteristics of the ellipsoid particle packing, and found some interesting microstructure evolution laws of ellipsoid granular packing. However, the strain controlled loading method in Ng's engine is not as stable as stress controlled technique, and the generated granular sample is far away from real granular matter. Thornton [19] studied the evolution of strain under loading in deviatoric stress plane, and proved that Lade criterion is appropriate for considering the influence of intermediate principal stress on the strength of granular materials of spherical packing. Later, Thornton [20] studied stress behavior and fabric evolution characteristics under loading in deviatoric strain plane. But Thornton's study also ignored the real granular matter effect.

As summarized above, most previous researches by DEM were focused on mechanical behavior of granular material under axisymmetric loading. And yet, very limited studies were concerned with complex stress loading, especially for real granular material. Those fundamental studies mainly paid attention to new particle shape or new contact law, almost without noticing real granular material and 3D stress effects. On the other hand, DEM simulation in geotechnical engineering usually depended on simple contact model and primary calibration. As a result, it is a genuine pressing task for DEM users to consider both complicated loading path and meticulous calibration along with non-spherical effects of particles for either fundamental studies or engineering applications.

The target of this study is justified by foregoing expounding to develop a numerical true axial engine capable of providing elastic-plastic behavior in 3D stress states for real granular material. The arrangement of this work is as below. Firstly, DEM considering rolling resistance is introduced to establish a numerical true axial engine. Then, the new engine is applied to simulate the behavior under different loading path in both deviatoric stress plane and meridian stress plane. Later, some typical strength criteria are examined with respect to the cohesionless granular material we have studied. Finally we finish the article by a few conclusions.

2. Numerical true triaxial engine

Original spherical particle model excludes rolling resistance, resulting in larger simulated dilatancy than the experiment data in triaxial compression [11]. When simulating real granular media, the moment transmitted must be introduced to handle the non-spherical effects. Therefore, we add a rolling resistance in the contact model as below.

2.1. Contact model

As shown in Fig. 1, the radii of the two contacting particle A and B are represented by R_A and R_B with the normal overlap ΔU_n Then, we are able to calculate the normal and shear forces via Eqs. (1) and (2)

$$F_n = k_n \Delta U_n \tag{1}$$

$$\Delta F_s = -k_s \Delta U_s \tag{2}$$

where k_n and k_s are normal and shear stiffness, respectively. By using the conventional parametrization approach in Yade community, the particle contact modulus Y and stiffness ratio $\alpha = \frac{k_s}{k_n}$, $k_n = 2\frac{Y \cdot R_A \cdot R_B}{(R_A + R_B)}$ are used to define the normal and tangential stiffness.

Granular material is a friction matter, so the shear force $F_s$must be less than a threshold. As usual, the Coulomb friction law is used to model contact friction as show in Eq. (3).

$$F_s \leqslant \mu |F_n| \tag{3}$$

where μ is the particle friction coefficient, $\mu = \tan(\Phi)$, Φ is the friction angle.

We use our former rolling resistance moment model [11] for spherical particle to consider the real particle shape effect. M is the rolling resistance moment, θ_r is the relative rotation angle between two contacting particles, and k_r is the rolling stiffness, so the rolling resistance moment can be written via Eq. (4).

$$M = k_r \cdot \theta_r \tag{4}$$

It is convenient to use a dimensionless number β_r to define the rolling stiffness as $k_r = \beta_r R_A R_B k_s$.

2.2. Numerical true triaxial apparatus

Based on the rolling contact model, a numerical true triaxial apparatus is established. Fig. 2 demonstrates the whole computational procedures of the stress controlled true triaxial apparatus. Firstly, a cuboid cell with six walls to be filled with particles is formed for loading. The radius expansion approach is used to

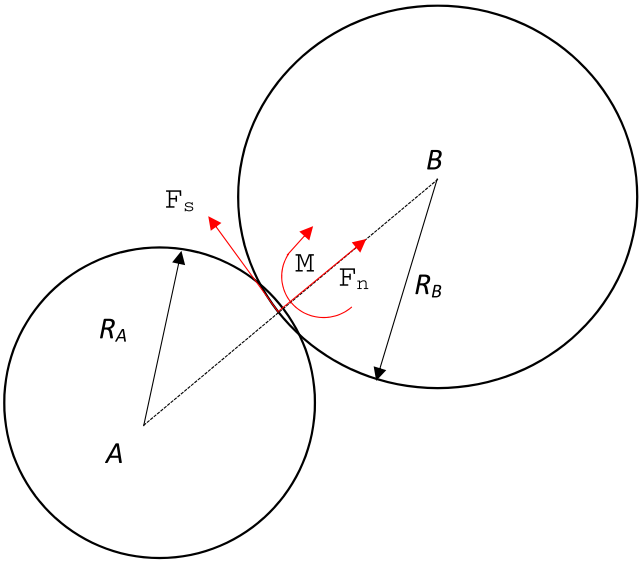

Fig. 1. Two spheres in contact.

Please cite this article as: X. Wang, Z. Zhang and J. Li, Triaxial behavior of granular material under complex loading path by a new numerical true triaxial engine, Advanced Powder Technology, https://doi.org/10.1016/j.apt.2018.12.020

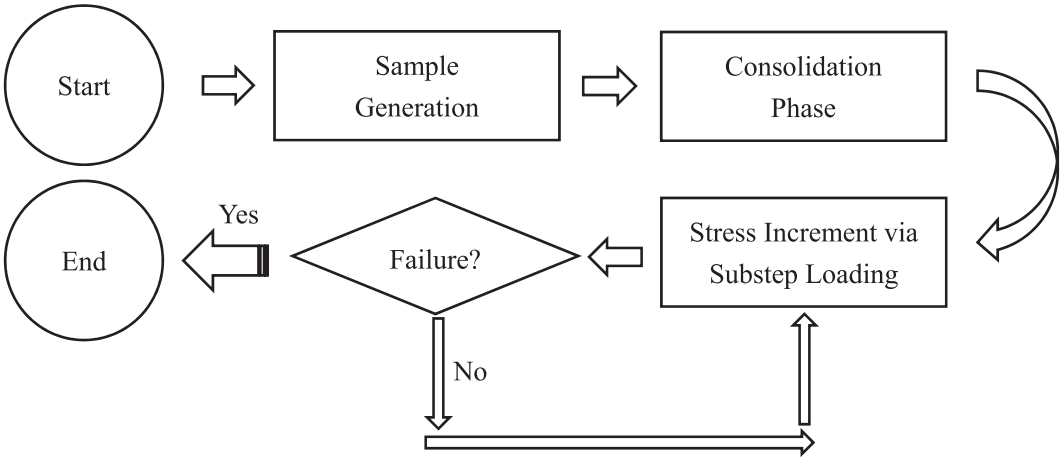

Fig. 2. Computational procedures of the numerical true triaxial engine.

generate a uniform sample in bulk with controlled anisotropy only near the wall. Then, consolidation is continued by moving the six walls towards the cell center before a specified confining stress is realized. Finally, the prepared sample is under loading according to the specified stress path until failure. The stress path can be decomposed into a series of steps, with each step divided into a series of sub-steps to maintain the sample in quasi-static state during loading. Two main classes of loading schemes are designed, including stress paths on meridian stress plane passing through hydrostatic axis as shown in Fig. 3 where $\sigma_2 = \sigma_3$, and deviatoric stress paths on plane perpendicular to the hydrostatic axis as shown in Fig. 3 where $\sigma_1 + \sigma_2 + \sigma_3 = constant$ and σ_1, σ_2 and σ_3 are three principal stresses respectively. Our stress-controlled numerical engine is capable to manipulate stress increment accurately and maintain constant of stress path, as compared to Ng's strain controlled engine [14,18]. The stress-controlled numerical true triaxial apparatus is able to simulate the hardening behavior, but unable to model the softening behavior. Actually, the numerical stress controlled true triaxial apparatus is established via a series Python subroutines on the platform of Yade (version 0.90) [21].

2.3. Verification by conventional triaxial loading case study

The 4 microscopic contact parameters of this rolling model should be calibrated before modeling real granular material. The relationship between the 4 microscopic parameters and macroscopic mechanical behavior is carefully studied in [11], and a calibration technique is provided for real granular material. The 4 microscopic parameters determine 4 key macroscopic parameters (Young' s modulus, Poisson's ration, Friction angle, and Dilatancy angle). Thus the DEM model was established for Chende sand [11] with the 4 contact parameters calibrated via the calibration technique in [11] as listed in Table 1. The consolidated drained triaxial compression tests under confining stresses of 100 kPa and 300 kPa are well conducted by the new numerical true triaxial engine. The simulated results are shown in Figs. 4 and 5. We find that the peak strength, dilatancy behavior, and the hardening behavior agree well with the experiments. Hence, we believe that the new numerical true triaxial engine really possesses the ability of conventional triaxial compression engine in simple stress-controlled paths. Then it is used to study the mechanical response in other 3D loading cases.

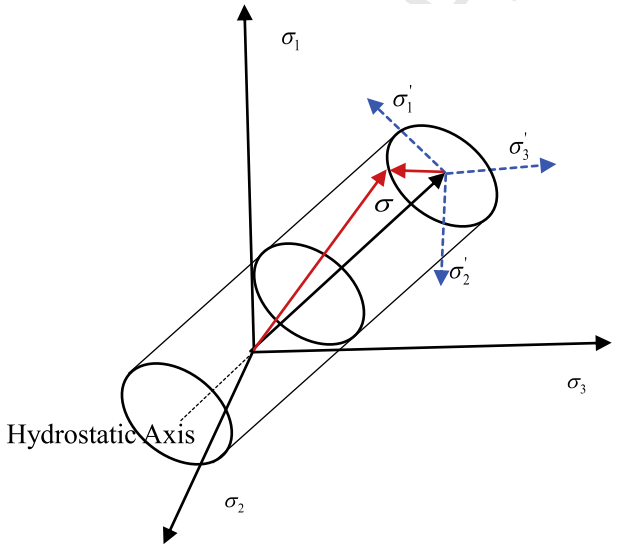

Fig. 3. Illustration of principal stress space.

3. Mechanical behavior in meridian stress space

3.1. Stress path

The axisymmetric loading path lies in the meridian stress plane through hydrostatic axis as shown in Fig. 3, where $\sigma_2 = \sigma_3$. Firstly, the sample is consolidated to a mean pressure of 300 kPa, then the sample is loaded along five different loading paths in the meridian plane, until the sample fails. The five loading paths in the meridian stress plane are show in Fig. 6.

CD represents consolidated drained compression, in which, lateral pressure is kept constant, and the axial stress is increased until sample fails. CMS means constant mean stress compression, where the mean pressure is kept constant when axial stress is increased until sample fails. LE means lateral extension, in which axial stress is kept constant, while lateral stress is decreased until sample fails. AE is axial extension, in which, lateral stress is kept constant, while axial stress is decreased until sample fails. LC denotes lateral compression, in which axial stress is kept constant, while lateral stress is increased until sample fails. During the loading process, if the

Table 1
Contact parameters of Chende sand.

Item	Value
Contact modulus Y (MPa)	800
Stiffness ratio α	0.1
Inter-particle friction angle Φ	22°
Rolling resistance coefficient β_r	0.6

Please cite this article as: X. Wang, Z. Zhang and J. Li, Triaxial behavior of granular material under complex loading path by a new numerical true triaxial engine, Advanced Powder Technology, https://doi.org/10.1016/j.apt.2018.12.020

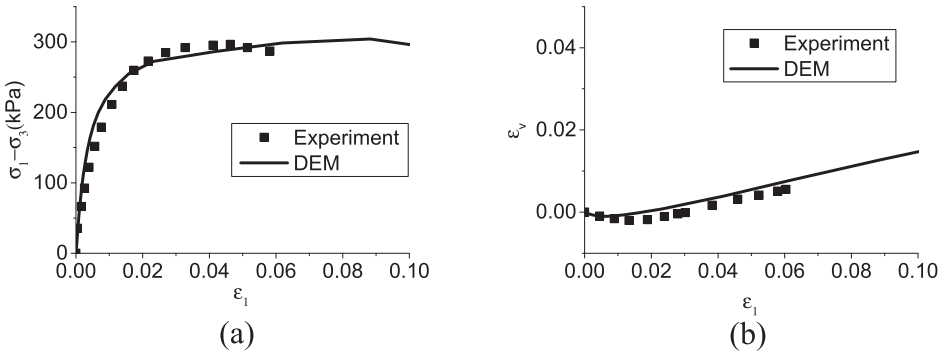

Fig. 4. Triaxial response of both DEM model and experiments under confining pressure 100 kPa. (a) Stress strain behavior. (b) Volume strain versus axial strain.

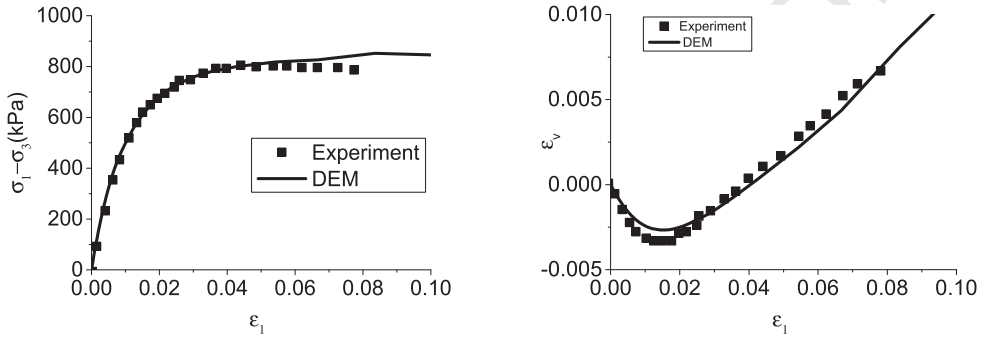

Fig. 5. Triaxial response of both DEM model and experiments under confining pressure 300 kPa. (a) Stress strain behavior. (b) Volume strain versus axial strain.

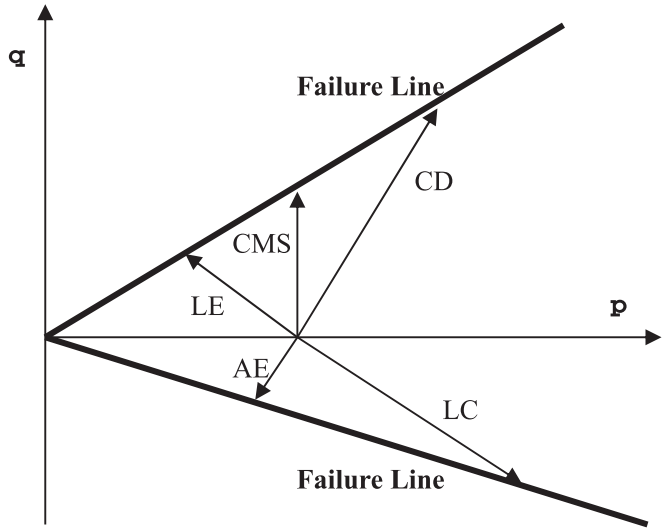

Fig. 6. Stress loading paths in meridian plane.

general shear strain defined below in 3.2 is larger than 10%, then loading is finished.

3.2. Simulated results

The stress and strain in three directions are monitored during the loading. The general shear stress and general strain defined in Eqs. (5) and (6) are used to describe the mechanical response.

$$q = \sqrt{\frac{(\sigma_1-\sigma_2)^2+(\sigma_2-\sigma_3)^2+(\sigma_1-\sigma_3)^2}{2}} \quad (5)$$

$$\varepsilon_q = \frac{\sqrt{2}}{3}\sqrt{(\varepsilon_1-\varepsilon_2)^2+(\varepsilon_2-\varepsilon_3)^2+(\varepsilon_1-\varepsilon_3)^2} \quad (6)$$

In conventional triaxial compression tests, the expression of general stress and general strain returns back to the formulae used in soil mechanics, as shown in Eqs. (7) and (8).

$$q = \sigma_1 - \sigma_3 \quad (7)$$

$$\varepsilon_q = \frac{2}{3}(\varepsilon_1 - \varepsilon_3) \quad (8)$$

The general shear stress and general strain curve response or the volume strain response are shown in Fig. 7 or Fig. 8, respectively.

From Figs. 7 and 8, the DEM model is able to simulate the mechanical responses under complex loading path if calibrated against simple loading path at first. Fig. 7 shows that stress strain response considerably depends on loading path in meridian plane. The general shear stress of CD is larger than any other loading path, while the general shear stresses of AE and LC are the smallest among the five cases, and close to each other. Fig. 8 indicates that the dilatancy also depends on loading path in meridian stress plane. Volume strain of CD exhibits a combination of first compression and then expansion during loading process, which is shared by LC. However, there is almost no volume contraction process for CMS, AE and LE, which should be attributed to no hydrostatic pressure growth in these cases.

4. Mechanical behavior in deviatoric stress space

4.1. Stress path

In the deviatoric stress plane perpendicular to hydrostatic axis as shown in Fig. 3, there are six sections divided by the three principal stress lines and their extensions like in Fig. 9. Because of sym-

Please cite this article as: X. Wang, Z. Zhang and J. Li, Triaxial behavior of granular material under complex loading path by a new numerical true triaxial engine, Advanced Powder Technology, https://doi.org/10.1016/j.apt.2018.12.020

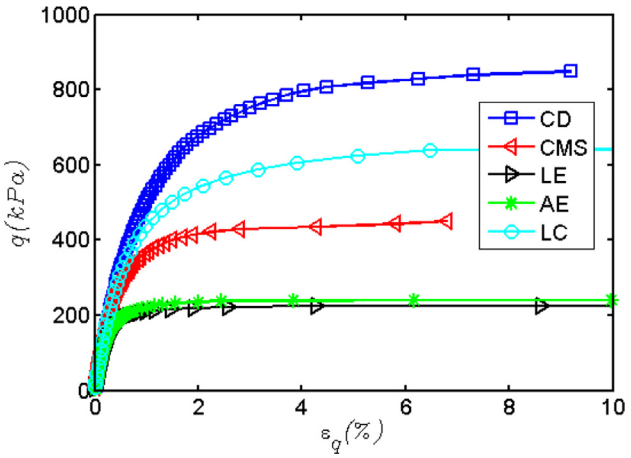

Fig. 7. General shear stress versus general shear strain for five different loading paths in meridian stress plane.

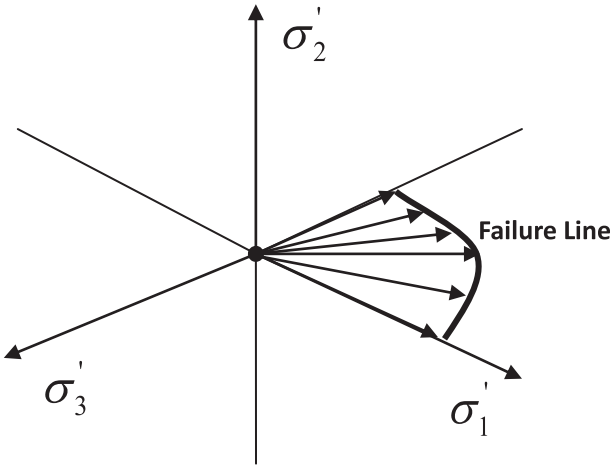

Fig. 9. Stress paths in deviatoric stress plane.

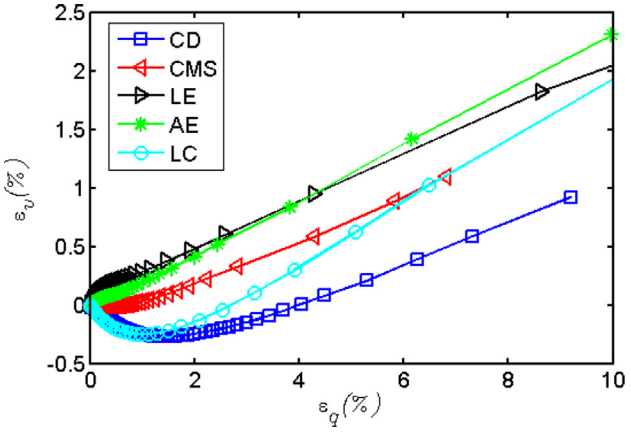

Fig. 8. Volume strain versus general shear strain for the five different loading paths in meridian stress plane.

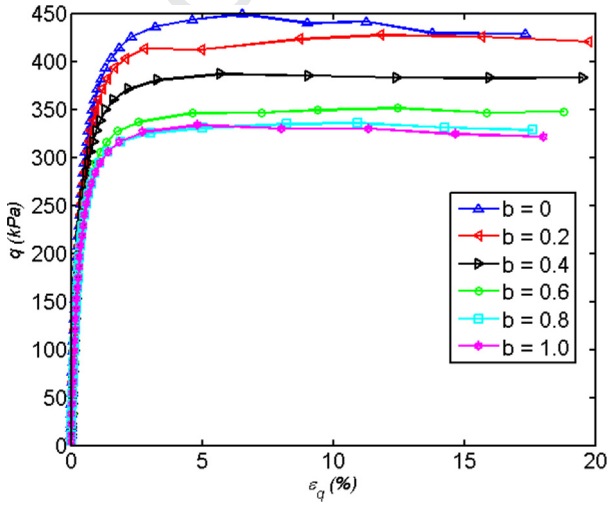

Fig. 10. General shear stress versus general shear strain responses for the six loading paths in the deviatoric stress plane. Mean stress is 300 kPa.

metry, only one of sixth part of the deviatoric plane where $\sigma_1 \geqslant \sigma_2 \geqslant \sigma_3$ is considered. All of the symbols in this part follow the convention in soil mechanics, where positive sign denotes compressive stress. Every b with definition of $b = \frac{\sigma_2 - \sigma_3}{\sigma_1 - \sigma_3}$ corresponds to a Lode angle on deviatoric stress plane. Six cases with different loading paths where b is 0, 0.2, 0.4, 0.6, 0.8 and 1.0, as shown in Fig. 9, are simulated. The case $b = 0.0$ corresponds to CD, and that $b = 1.0$ corresponds to AE.

Firstly, the sample is consolidation to mean pressure of 300 kPa. Then the sample is loaded along the six loading paths in Fig. 9 until failure. During the loading process, mean pressure and b are kept constant, when the general shear strain is larger than 20%, the loading is finished.

4.2. Simulated results

The general shear stress versus general strain curve response is shown in Fig. 10, and the volume strain response is shown in Fig. 11.

Fig. 10 indicates that all the mechanical responses of the six loading paths are hardening type. The general shear stress shows initial increases, and then gradually approaches to a constant state. If b is larger, the general shear stress in failure is smaller correspondingly. Fig. 11 indicates that, if b is larger, dilatancy angle is larger. There is no initial compression phase because of mean pressure are kept constant during loading for all the cases.

5. Theoretical analysis and discussion

Modeling strength property of geomaterial, such as soil, rock and concrete, is more difficult than metal. Due to the complex mathematical operation of 3D problems in tensor analysis, people prefer to develop strength criterion in 2D space at first, and then extends the results into 3D stress space via stress transformation. However, the DEM analysis obviously suggested that 3D effects such as intermediate stress states is significant and should be considered in the strength criterion. At this moment, we would firstly use two simpler strength criteria in 3D stress space rather than Lade-Ducan and Matsuoka-Nakai criteria. The two criteria including Yu's unified strength theory (UST) criterion and van Eekelen's (VE) strength criterion are examined in the following:

5.1. Two strength criteria for granular material

UST criterion is proposed by Yu [5]. This criterion is composed of a piecewise of linear lines, parameters determined by experi-

Please cite this article as: X. Wang, Z. Zhang and J. Li, Triaxial behavior of granular material under complex loading path by a new numerical true triaxial engine, Advanced Powder Technology, https://doi.org/10.1016/j.apt.2018.12.020

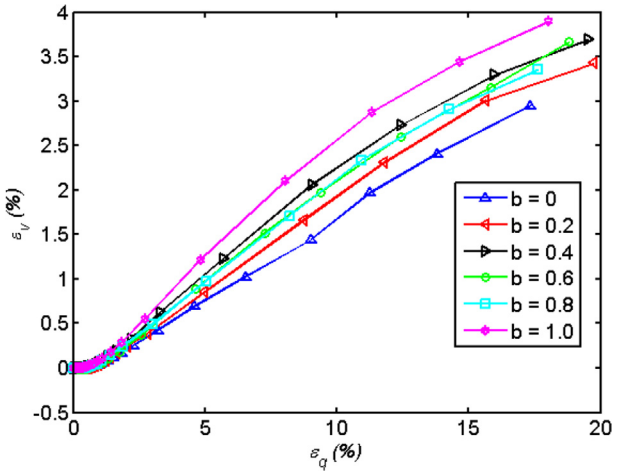

Fig. 11. Volume strain versus general shear strain responses for the six loading paths in deviatoric stress plane. Mean stress is 300 kPa.

ments easily. UST has found numerous applications in the strength and constitutive modeling of metal, rock, concrete and soil. The UST criterion composed of two linear lines in principal stress space can be written in Eq. (9) as below;

$$\begin{cases} F = \sigma_1 - \frac{\alpha_1}{1+B}(B\sigma_2 + \sigma_3) = 0 & \sigma_1 + \alpha_1\sigma_3 \geqslant (1+\alpha_2)\sigma_2 \\ F' = \frac{1}{1+B}(\sigma_1 + B\sigma_2) - \alpha_2\sigma_3 = 0 & \sigma_1 + \alpha_1\sigma_3 < (1+\alpha_2)\sigma_2 \end{cases} \quad (9)$$

where $\sigma_1 \geqslant \sigma_2 \geqslant \sigma_3$, $\alpha_1 = \left(\frac{1+\sin\varphi}{1-\sin\varphi}\right)_{compression}$, $\alpha_2 = \left(\frac{1+\sin\varphi}{1-\sin\varphi}\right)_{extension}$. σ_1, σ_2 and σ_3 are principal stresses. B is a parameter between 0 and 1.

Van Eekelen proposed another strength criterion for granular material in 1980 [4]. VE criterion is established in the cylindrical coordinate system of principal stress space. The general formula is shown in Eq. (11).

$$\frac{r}{p+c} = f(p)g(\theta) \quad (11)$$

where r denotes radius in deviatoric stress plane, and $r = \sqrt{\frac{2}{3}}q$, c denotes cohesion, and θ is Lode angle (angle between stress vector and the horizontal line in deviatoric plane as in Fig. 3). As for the special case of cohensionless granular matter, the general formula is specified as a 3-parameters-based criterion in Eqs. (12) and (13).

$$\frac{r}{p} = g(\theta) \quad (12)$$

$$g(\theta) = \alpha(1 - \beta sin(3\theta))^n \quad (13)$$

5.2. Model performance

From the triaxial compression (b=0) results, and trixial extension (b=1.0) results in deviatoric stress plane, the parameters α_1 = 4.158 and α_2 = 5.278 of UST criterion are produced, respectively. By conventional data fitting in different Lode angles, B is determined as 0.5. Thus the strength envelope in deviatoric stress plane of mean stress of 300 kPa is shown in Fig. 12 by dashed line.

Through careful data fitting for all cases of different Lode angles under hydrostatic stress of 300 kPa, we finally obtain parameters for VE criterion. α is 0.985, β is −0.85 and n is −0.123. The envelope of VE criterion is shown in Fig. 12 as the green line.

The two-parameter-based criteria of DP and MC widely used in engineering are also shown in Fig. 12. The parameters in MC criterion are determined by triaxial compression tests while those in DP criterion is found by the tests passing through the outer corner of MC criterion with the DP circle on deviatoric stress plane. The symbols in red denote the strength of the six different loading paths on deviatoric stress plane. From Fig. 12, the UST criterion and VE criterion are found to coincide with the DEM results very well. On the other hand, VE criterion is smooth in all directions, however UST is a combination of twelve lines. Fig. 12 further demonstrates that MC criterion underestimates the strength in deviatoric stress plane except for triaxial compression, while DP criterion overestimates the strength. Both DP and MC criterion have exhibited some drawbacks in modeling granular materials under 3D loading.

The envelopes of UST, VE, MC and DP in meridian plane are displayed in Fig. 13. It is found in the region of triaxial compression, the four criteria coincide very well with each other. However, some deviations are found in the region of triaxial extension: MC prediction is smaller than the DEM results, DP prediction is larger than DEM results, while UST and VE criteria agree well with the DEM results. The prediction of MC criterion is closer to DEM simulation result than DP in the triaxial extension region.

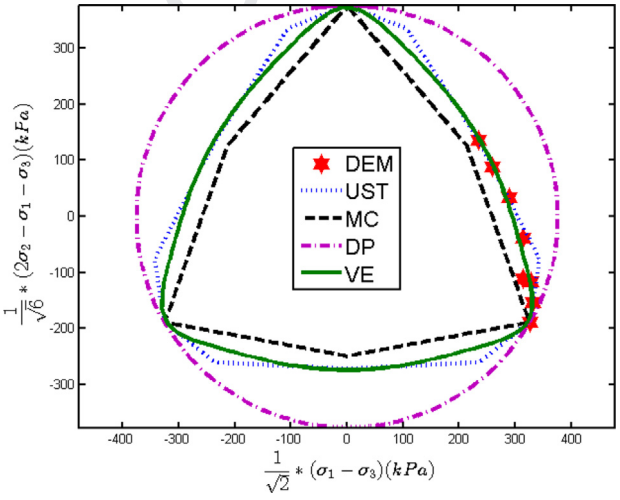

Fig. 12. Envelopes of unified strength theory, van Eekelen, Mohr-Coulomb and Drucker-Prager criteria in deviatoric stress plane of mean pressure of 300 kPa, the red symbols denote the DEM results. (For interpretation of the references to colour in this figure legend, the reader is referred to the web version of this article.)

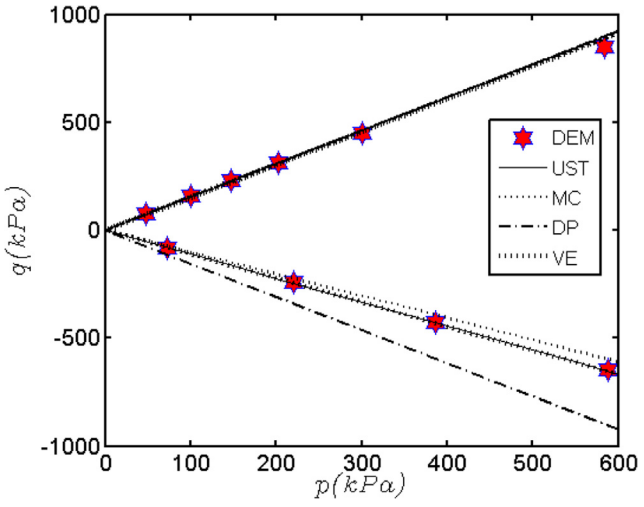

Fig. 13. Envelopes of unified strength, van Eekelen, Mohr-Coulomb and Drucker-Prager criteria in meridian stress plane, the pink symbols denote the DEM results. (For interpretation of the references to colour in this figure legend, the reader is referred to the web version of this article.)

Please cite this article as: X. Wang, Z. Zhang and J. Li, Triaxial behavior of granular material under complex loading path by a new numerical true triaxial engine, Advanced Powder Technology, https://doi.org/10.1016/j.apt.2018.12.020

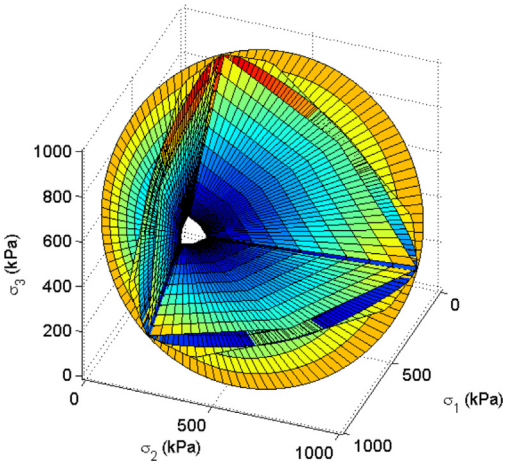

Fig. 14. Envelopes of the four strength criteria. Surfaces from outer to inner denote DP, UST, VE and MC criteria respectively.

Fig. 14 depicts the whole surfaces of UST, VE, MC and DP criteria in principal stress space. The surface of DP is a circular conical, the surface of MC is a six-sided pyramid, and surface of UST strength criterion is a 12-sided pyramids, while the surface between MC and UST is a duck egg conical surface.

6. Conclusion

Based on rolling contact discrete element model, a relatively stable stress controlled numerical true triaxial engine is developed to simulate the mechanical behavior of granular material in 3D stress space. Arbitrary stress path in both meridian plane and deviatoric plane can be specified to examine the stress-strain responses. Finally, we are able to come to the following conclusions:

(1) In the meridian plane: from same initial confining stress state, triaxial compression including CD, CMS and LE fails on a line passing through the origin, while the failure line of triaxial extension including AE and LC falls on another line, but the slope of which is smaller than MC theory prediction. Volume in mean pressure increasing loading case such as CD and LC firstly contracts, and then expands until failure, while volume in non-increasing pressure loading case including CMS, LE and AE always dilates until failure.
(2) In the deviatoric plane: the strength of triaxial compression is larger than any other loading scenarios, similarly, dilatancy of triaxial extension is also greater than others. It implies that the 3D effects such as intermediate principal stress should be taken into account in modeling granular materials in complex stress states.
(3) Two simplest strength criteria UST and VE with only three parameters, readily determined by the numerical true triaxial engine, are found to be capable of well modeling the strength behavior in 3D stress space for cohensionless granular material. While the classical DP and MC theory exhibits some deviation in predicting strength of granular matter in 3D stress space other than triaxial compression loading cases.
(4) The case study of Chende sand shows that the new developed numerical true triaxial engine, if well calibrated with reliable conventional triaxial compression tests for a typical granular material, is a potential technique to provide information of elastic-plastic behavior of granular material in 3D stress space. The numerical true triaxial engine developed in this study is proved to be helpful for further full FEM analysis in geotechnical and geological engineering. However, the issue of softening, constitutive behavior of silt and clay need further study through bonded particle model and more careful calibration.

Acknowledgement

The authors are grateful to the financial support by National Natural Sciences Foundation of China (No. 11602278, 11432015), National Key R&D Program of China (2018YFC1505504), and the Strategic Priority Research Program of Chinese Academy of Sciences (XDB22040203).

References

[1] D.M. Wood, Soil Behaviour and Critical State Soil Mechanics, Cambridge University Press, Cambridge, 1990.
[2] P. Lade, Elasto-plastic stress-strain theory for cohesionless soil with curved yield surfaces, Int. J. Solids Struct. 13 (2009) 1019–1035.
[3] H. Matsuoka, On the significance of the "spatial mobilized plane", Soils Found. 16 (1976) 91–100.
[4] V. Eekelen, Isotropic yield surfaces in three dimensions for use in soil mechanics, Int. J. Numer. Anal. Meth. Geomech. 4 (1980) 89–101.
[5] M.H. Yu, Unified Yield Criteria, Springer, Berlin Heidelberg, 2004.
[6] P.A. Cundall, O. Strack, A discrete numerical model for granular assemblies, Geotechnique 29 (1979) 47–65.
[7] G. Gong, X. Zha, J. Wei, Comparison of granular material behaviour under drained triaxial and plane strain conditions using 3D DEM simulations, Acta Mech. Solida Sin. 25 (2012) 186–196.
[8] M.R. Kuhn, Micro-mechanics of fabric and failure in granular materials, Mech. Mater. 42 (2010) 827–840.
[9] K. Iwashita, M. Oda, Micro-deformation mechanism of shear banding process based on modified distinct element method, Powder Technol. 109 (2000) 192–205.
[10] M.J. Jiang, H.S. Yu, D. Harris, A novel discrete model for granular material incorporating rolling resistance, Comput. Geotech. 32 (2005) 340–357.
[11] X.L. Wang, J.C. Li, Simulation of triaxial response of granular materials by modified DEM, Sci. China Phys. Mech. Astron. 57 (2014) 2297–2308.
[12] C. Salot, P. Gotteland, P. Villard, Influence of relative density on granular materials behavior: DEM simulations of triaxial tests, Gran. Matter 11 (2009) 221–236.
[13] G. Saussine, C. Cholet, P.E. Gautier, Modelling ballast behaviour under dynamic loading. Part 1: A 2D polygonal discrete element method approach, Comput. Meth. Appl. Mech. Eng. 195 (2006) 2841–2859.
[14] T.T. Ng, Macro-and micro-behaviors of granular materials under different sample preparation methods and stress paths, Int. J. Solids Struct. 41 (2004) 5871–5884.
[15] L. Scholtès, B. Chareyre, F. Nicot, Micromechanics of granular materials with capillary effects, Int. J. Eng. Sci. 47 (2009) 64–75.
[16] X.L. Wang, J.C. Li, A novel liquid bridge model for estimating SWCC and permeability of granular material, Powder Technol. 275 (2015) 121–130.
[17] X. Zhao, T.M. Evans, Numerical analysis of critical state behaviors of granular soils under different loading conditions, Granul. Matter 13 (2011) 751–764.
[18] T.T. Ng, Behavior of gravity deposited granular material under different stress paths, Can. Geotech. J. 42 (2005) 1644–1655.
[19] C. Thornton, S.J. Antony, Quasi-static shear deformation of a soft particle system, Powder Technol. 109 (2000) 179–191.
[20] C. Thornton, L. Zhang, On the evolution of stress and microstructure during general 3D deviatoric straining of granular media, Géotechnique 60 (2010) 333–341.
[21] V. Šmilauer, E. Catalano, B. Chareyre, Yade reference documentation, Yade Document. (2010).